Int. J. Environ. Sci. Technol. (2016) 13:865–874
DOI 10.1007/s13762-015-0914-y

ORIGINAL PAPER

Incorporation of chitosan and glass substrate for improvement in adsorption, separation, and stability of TiO_2 photodegradation

M. N. I. Amir[1] · N. M. Julkapli[1] · S. B. Abd Hamid[1]

Received: 2 September 2015 / Revised: 27 October 2015 / Accepted: 30 November 2015 / Published online: 4 January 2016

Abstract It is demonstrated that single titanium dioxide (TiO_2) has high potential for photodegradation of pollutants. However, it is still far from becoming an effective photocatalyst system, due to issues of adsorption process, separation, as well as dissolution. Therefore, this study highlights the high adsorption capacity, simplified separation, and the promising stability of $TiO_{2(SY)}$ (synthesized via sol–gel method) photocatalyst, fabricated using chitosan–$TiO_{2(SY)}$ and supported by glass substrate (Cs–$TiO_{2(SY)}$/glass substrate) photocatalysts. Chitosan (Cs), with abundant –R–NH and NH_2 groups, promotes the adsorption sites of methyl orange (MO) and OH groups for major attachment to $TiO_{2(SY)}$. Meanwhile, the glass substrate increases stability and assists separation of the photocatalysts. Initially, nano-$TiO_{2(SY)}$ has been characterized using high-resolution transmission electron microscope. Cs–$TiO_{2(SY)}$/glass substrate was fabricated via dip-coating. The distribution and interface between the photocatalytic components were characterized by Fourier transform infrared absorption spectroscopy, UV–Vis diffuse reflectance spectroscopy, field emission scanning electron microscopy, and energy-dispersive spectrometer. UV–Vis analysis of the multilayer photocatalyst (2, 4, 6, and 8 layers) was further carried out by the adsorption–photodegradation, with MO as model of pollutant. Seventy percent of the total removal of MO via optimized eight layers of photocatalyst was achieved within 1 h of UV irradiation. The adsorption photocatalyst achieved 50 % with no exposure to UV light for 15 min of irradiation. It is concluded that suitable photocatalytic conditions and sample parameters possessing the multilayer photocatalyst of Cs–$TiO_{2(SY)}$ are beneficial toward the adsorption–photodegradation process in wastewater treatment.

Keywords Adsorption–photodegradation · Methyl orange · Titanium dioxide · Chitosan · Glass substrate

Introduction

One of the major sources of water contamination is the textile industry, due to its heavy usage of various synthetic and organic dyes (Liu et al. 2004; Pereira and Alves 2012). Various methods have been used to treat synthetic dyes, such as adsorption by various adsorbents, reverse osmosis, and flocculation. These methods are commonly used in wastewater treatment facilities, and among them, photocatalysis stands out due to its environmental-friendly nature, cost-effectiveness, and the lack of the production of secondary pollutants after the degradation of dyes.

Titanium dioxide (TiO_2) nanoparticles, or nano-TiO_2 with one-dimensional structure, is a well-known semiconductor used as a photocatalyst, due to its chemical structure, biocompatibility, physical properties, catalytic activity, high surface area, non-toxicity, and promising electroconductivity (Fujishima 1972; Kijima 2010). However, nano-TiO_2 is still far from becoming a potential candidate for photocatalyst systems. Bundling phenomenon and weak adherence due to the multiphase nature of TiO_2 substrate remain a great challenge. Moreover, poor visible light absorption and rapid recombination of charge carriers limit the widespread use of TiO_2. Therefore, the

✉ N. M. Julkapli
nurhidayatullaili@um.edu.my

[1] Nanotechnology and Catalysis Research Centre (NANOCAT), 3rd Floor, Block A, Institute of Postgraduate Studies (IPS), University of Malaya, 50603 Kuala Lumpur, Malaysia

donor and acceptor molecules must reach the catalyst surface prior to recombination (Gupta et al. 2012). Nano-TiO_2 can be also easily suspended in water, clog filter membranes, and penetrate filter materials, which create problems to the separation process at the end of wastewater treatment.

Chitosan (Cs) is a biopolymer that is highly stable, and represents an idealized structure of adsorbent materials, due to its R–OH, $–RNH_2$, and R–NH–R structures (Dutta et al. 2004). It was reported that Cs effectively adsorbs synthetic dyes, metal ions, organic acids, and pesticide from various types of wastewater. Meanwhile, protonation of $R–NH_2$ or R–OH functional groups of Cs in acidic medium helps form a good interface with nano-metal oxide. This shows the high potential of Cs as a support material for nano-metal oxide particles, resulting in its uniform distribution within the Cs matrix. Moreover, the use of Cs represents a promising and effective alternative as opposed to other traditional wastewater treatment methods, such as activated carbon adsorption, biological treatment, and flocculation (Zainal et al. 2009). However, Cs is soluble in acidic medium ($pKa < 4.6$), which limits its application in highly concentrated H^+ ion solutions (Wongkupasert 2008).

The adsorption process involves two items: adsorbent and adsorbate, corresponding to the solid surface and pollutant that sticks to the solid surface, respectively. Adsorption is affected by the nature of adsorbates and adsorbents, the presence of other pollutants, temperature, and other atmospheric and experimental conditions. Moreover, other factors also control adsorption, such as particle size of the adsorbent, temperature, pH, contact time, and concentration of pollutants (Ali 2010, 2012, 2014). This is important in the context of water treatment, as it uses low-cost adsorbent, resulting in a positive effect toward waste management. Moreover, management of low-cost adsorbents is an alternative that can prove inexpensive for commercialization. However, the management of the exhausted adsorbent is an important issue and has not been addressed completely. There is a need to develop more efficient, selective, inexpensive, and eco-friendly low-cost adsorbents to treat wastewater. Briefly, there is a demand for a module of low-cost adsorbents that are fast-acting and eco-friendly (Ali et al. 2012).

Promising fabrication methods have been proposed for efficient separation and adsorption of TiO_2/Cs photocatalysts, including TiO_2/Cs beads, TiO_2/Cs multilayers, TiO_2/Cs composites, TiO_2/Cs composite on cotton fibers, TiO_2/Cs with SiO_2 support and TiO_2/Cs-activated carbon, and TiO_2/Cs with ZnO nano-composite thin films (Jawad and Nawi 2012; Kim et al. 2005; Qian et al. 2011; Yu et al. 2014; Zhang et al. 2011; Zhu et al. 2012). One proposed method is the preparation of TiO_2/Cs hybrid film onto substrate materials. In this approach, the photocatalyst can be separated from the reaction medium by just taking out the glass substrate from the solution.

This report discusses the photocatalytic activity of multilayer porous photocatalyst of $TiO_{2(SY)}$ within Cs matrix on the glass substrate. Unlike previous studies of using single TiO_2 or TiO_2/Cs photocatalysts, the presence of glass substrates is expected to promote better stability and higher surface area of the photocatalyst system and to simplify separation after treating the photocatalyst using irradiation. In this photocatalyst system, each layer of Cs–$TiO_{2(SY)}$ photocatalyst was sandwiched in order to fabricate 2, 4, 6, and 8 layers. Thus, the adsorption of synthetic dye molecules, as well as the photocatalytic activities of Cs–$TiO_{2(SY)}$/glass substrate, is expected to be more positive, mostly by bringing more dye molecules of methyl orange (MO) closer to the photocatalyst within the multilayers of the glass substrate.

Materials and methods

Materials

In the present study, commercial titanium isopropoxide (purity 97 %), $Ti[OCH(CH_3)_2]_4$, was used as the titanium precursor, while acetic acid (purity 99 %), CH_3CO_2H, was obtained from Sigma-Aldrich for the synthesis of $TiO_{2(SY)}$. Commercial Cs (medium molecular weight) and sodium chloride, NaCl, were obtained from Sigma-Aldrich and Merck, respectively, to prepare Cs–$TiO_{2(SY)}$ photocatalyst. MO was purchased from Sigma-Aldrich and used as the model pollutant to measure photocatalytic activity. Deionized water was used for preparing all standard solutions.

Fabrication of Cs–$TiO_{2(SY)}$/glass substrate photocatalyst

The fabrication of Cs–$TiO_{2(SY)}$/glass substrate began with the preparation of a Cs–$TiO_{2(SY)}$ photocatalyst solution. Cs flake (0.25 g) was dissolved in a premixed solution of CH_3COOH (30 ml; 0.1 M) and sodium chloride (NaCl) (4 ml; 0.2 M). The viscous solution was stirred continuously for 12 h before $TiO_{2(SY)}$ powder (0.25 g) was added. Subsequently, CH_3COOH (5 ml; 0.1 M) was added again, and stirring was continued for 24 h. Then, glass substrates ($25 \times 75 \times 2$ mm) were dipped in the Cs–$TiO_{2(SY)}$ photocatalyst viscous solution with uniform immersion and dried at 100 °C for 4 h alternately after each dipping process. The process was repeated to deposit 2, 4, 6, and 8 layers of Cs–$TiO_{2(SY)}$ photocatalyst onto the glass substrate.

Characterization of $TiO_{2(SY)}$ and Cs–$TiO_{2(SY)}$/glass substrate photocatalyst

The prepared $TiO_{2(SY)}$ was characterized using a JEM-2100F high-resolution transmission electron microscope (HR-TEM) at an accelerating voltage of 200 kV. The prepared $TiO_{2(SY)}$ and Cs on the glass substrate, namely Cs–$TiO_{2(SY)}$/glass substrate, were characterized using Fourier transform infrared absorption spectroscopy (FTIR), UV–Vis diffuse reflectance spectroscopy (UV-DR), and field emission scanning electron microscopy + energy-dispersive spectrometer (FESE-M + EDS) analysis at 4 cm^{-1} with 16 scans, in the wavelength range 400–4000 cm^{-1} of FTIR spectrum (Perkin-Elmer 100 spectrophotometer), providing molecular absorption and transmission (specific frequency of energy). FESEM analysis was done using scanning electron microscope (JSM-7500F, JEOL) at an acceleration voltage of 5 kV. The elemental analysis of the Cs–$TiO_{2(SY)}$/glass substrate of photocatalyst samples was conducted using EDS, with the energy of the beam in the range of 10–20 keV. The band gap energy analysis was conducted using UV-DR spectrophotometer model UV-3101PC Shimadzu, with wavelengths ranging from 200 to 800 nm.

Photocatalytic activity of Cs–$TiO_{2(SY)}$/glass substrate

A UV light lamp (6 W, $\lambda = 365$ nm) was used to initiate adsorption–photodegradation activity from prepared photocatalyst within a 150-ml Pyrex reactor containing 10 ppm MO. For the first 15 min, the sample was allowed to adsorb on the surface of the photocatalyst before being irradiated with a UV light lamp for the next hour. A sample of 5 ml was removed (including previous 15 min) at 10, 20, 30, 40, 50, and 60 min (Bagheri et al. 2015). The photocatalytic activity of Cs–$TiO_{2(SY)}$/glass substrate systems was usually evaluated by measuring the time dependence of the concentration loss based on adsorbed and degraded MO compound. MO is used due to its high stability and common UV–Vis spectroscopic profile under a variety of conditions, which encompasses the initial MO concentration, pH, photocatalyst dosage, and solar irradiation intensity. Furthermore, the absorbance data of the MO samples were obtained from the optical spectra recorded on UV–Vis analysis using model of UV-3101PC Shimadzu, with wavelengths ranging from 200 to 800 nm. After that, the multilayer photocatalyst was used with exactly similar photocatalytic activity from previous conditions as an evaluation parameter.

The percentage of adsorption–photodegradation was calculated using the following formula:

$$\%\,\mathrm{A{-}P} = \frac{C_o - C_t}{C_o} \times 100\,\% \quad (1)$$

where % A–P = percentage of adsorption and photodegradation; C_o = initial concentration of sample before irradiation under UV light; and C_t = concentration of sample after irradiation under UV light (t, minutes).

Results and discussion

Characterization of the synthesized $TiO_{2(SY)}$ photocatalyst

For HR-TEM analysis, the interaction of electrons with the specimen provides morphologic and compositional information of nano-materials. The prepared $TiO_{2(SY)}$ photocatalyst was characterized by HR-TEM analysis. The interaction of electrons with the specimen provides morphologic and compositional information of nano-$TiO_{2(SY)}$. The particle size and shape of the nano-sample are determined from the HR-TEM images shown in Fig. 1. The analysis is conducted based on the results reported in Fig. 2 and Table 1.

Figure 1 shows the HR-TEM images of the $TiO_{2(SY)}$ sample obtained after calcination at 500 °C. Generally, a homogenous dispersion and uniform particle feature, with particle sizes of 5–30 nm for $TiO_{2(SY)}$, are shown. It has been demonstrated that almost 90 % of the $TiO_{2(SY)}$ is 10–20 nm. Meanwhile, another 10 % of the $TiO_{2(SY)}$ has been categorized to be less than 5 nm or more than 25 nm.

Generally, 20 particles of $TiO_{2(SY)}$ had an average particle size of ~13.3 nm at a standard deviation of 7.2 nm, as depicted in Fig. 2 and Table 1. This result has been confirmed that $TiO_{2(SY)}$ was prepared via sol–gel method from the $Ti[OCH(CH_3)_2]_4$ precursor ($TiO_{2(SY)}$) which has an anatase phase. This implies that the repartition in size is quite large, i.e., 14 % of extension over the average value.

Characterization of the synthesized Cs–$TiO_{2(SY)}$/glass substrate photocatalysts

The Cs–$TiO_{2(SY)}$/glass substrate photocatalysts are characterized by FTIR, UV-DR, FESEM, and EDS. The FTIR spectrum provides the molecular absorption and transmission (specific frequency of energy), which is useful for analyzing the multilayer photocatalyst of Cs–$TiO_{2(SY)}$/-glass functional groups, while others are attached to the molecule's functional group, linking the photocatalyst with it. Characterization of FTIR spectra for formation of Cs–$TiO_{2(SY)}$/glass substrate multilayer photocatalyst together with single $TiO_{2(SY)}$ is shown in Fig. 3. Absorption bands at 1640 and 3600–3300 cm^{-1} are attributed to amide (R–

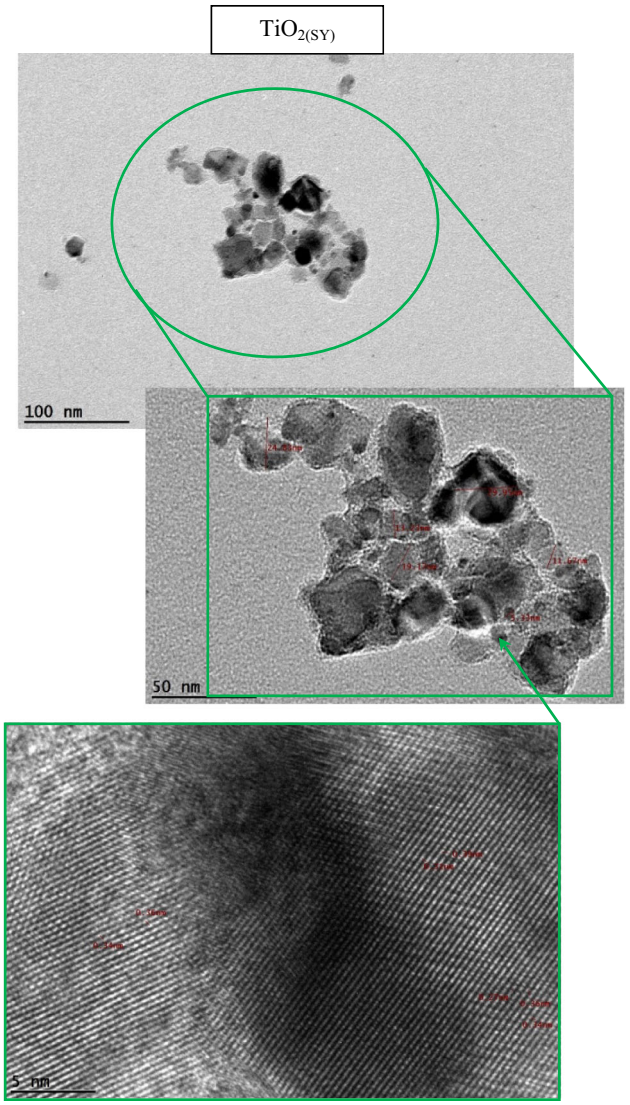

Fig. 1 HR-TEM micrographs of $TiO_{2(SY)}$ photocatalyst with magnification of ×60,000

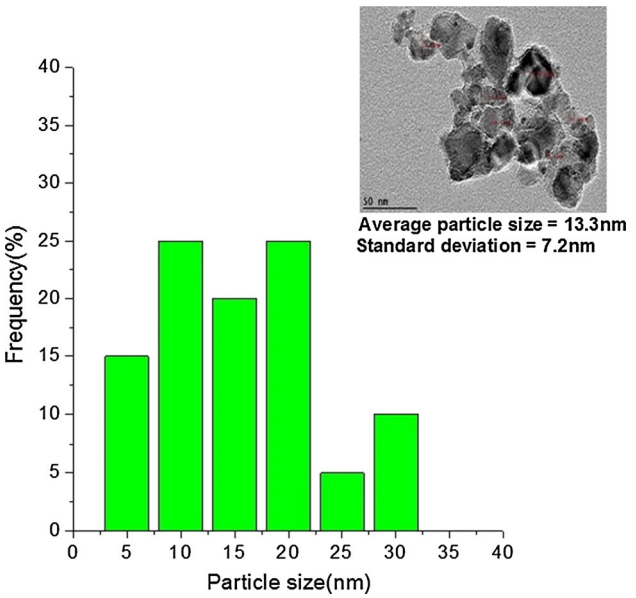

Fig. 2 PSD of $TiO_{2(SY)}$ (*green*) with inset at ×60,000 magnification

Table 1 Particle size and shape of $TiO_{2(SY)}$

Samples	Size (nm)	Shape		
		Cubic	Semi-sphere	Needle
Synthesis via sol–gel method				
$TiO_{2(SY)}$	13.3	A	N/A	N/A

N/A not available, *A* available

NH–R) and hydroxyl (–OH), together with amine ($–NH_2$) functional groups of Cs macromolecules for Cs–$TiO_{2(SY)}$/glass substrate. These series of functional groups on Cs chains serve as coordination and reaction sites for the adsorption of transition metals and organic species (Yao et al. 2011). The presence around the specific band at 700 cm^{-1} is assigned for Ti–O and Ti–O–Ti bonding of $TiO_{2(SY)}$ (Saleh and Gupta 2012a). However, there is an intriguing anomaly on the adsorption band of FTIR spectrum in the context of Cs–$TiO_{2(SY)}$ photocatalyst, which is due to the rough absorption bands of –OH group at 1400, 1535, 3420, and 3745 cm^{-1}, while the strong band at 3600–3300 cm^{-1} is attributed to characteristic of a surface TiO_2–OH group. On the other hand, the absorption bands at 1280–1070 cm^{-1} were attributed to the silicon–oxygen bonds (Si–O) functional groups. The significant increment in the bands was centered on 450–950 cm^{-1}, recorded for multilayer photocatalyst of Cs–$TiO_{2(SY)}$/glass substrate. The band increment became more significant as the number of layers from 2 to 8. It is worth noting that the FTIR spectra of the synthesized Cs–$TiO_{2(SY)}$ photocatalyst showed more bands with higher intensities compared with the precursor $TiO_{2(SY)}$ and Cs. It is indicated that the FTIR detection is enhanced when the photocatalysts consisted of both $TiO_{2(SY)}$ and Cs. Moreover, the apparent existence of NH_2, R–NH, and OH functional groups, together with $TiO_{2(SY)}$ metal oxide, should help confirm the effective removal of MO via the adsorption–photodegradation process. This can be explained by the adsorption of MO moleculars onto the Cs structure. Cs forms chelation between NH_2–MO and molecules–NH_2 within its long chain structure. It was previously proven that these functional groups act as adsorption sites and consequently increase the adsorption capacity of photocatalyst system (Kyzas and Bikiaris 2015).

UV-DR analysis was conducted to determine the band gap energy and absorption edge of the prepared Cs–TiO_2/glass substrate multilayer photocatalyst. Figure 4 presents the UV-DR spectra pattern for multilayer

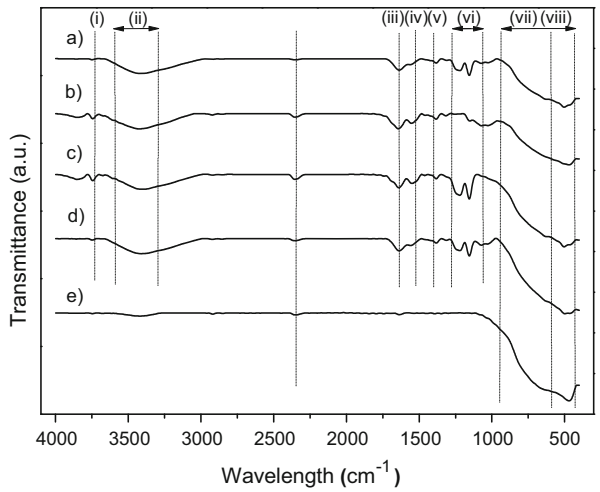

Symbol	Wavelength (cm^{-1})	Assignment
(i)	3745	–OH group
(ii)	3600 to 3300	–OH overlapping together with –NH_2 of Cs groups and –OH group to TiO_2 element attachment
(iii)	1640	R–NH–R bending
(iv) and (v)	1535 and 1400	–OH deformation
(vi)	1280 to 1070	Bridge of Si-O
(vii)	450 to 950	TiO_2 with shape of layers formation between Cs-$TiO_{2(SY)}$ on the glass substrate
(viii)	700	TiO_2 wagging

Fig. 3 FTIR spectra of Cs–$TiO_{2(SY)}$/glass substrate multilayers photocatalyst which are *a* 2 layers, *b* 4 layers, *c* 6 layers, and *d* 8 layers together with *e* $TiO_{2(SY)}$

photocatalyst of Cs–$TiO_{2(SY)}$/glass substrate. The band gap energy increased with layers from 2 to 4. It has demonstrated an increment in the band gap energy from 2.43 to 2.70 eV. The band gap decreases gradually from 4 layers until 8 layers at up to 0.96 eV. It can be anticipated that the

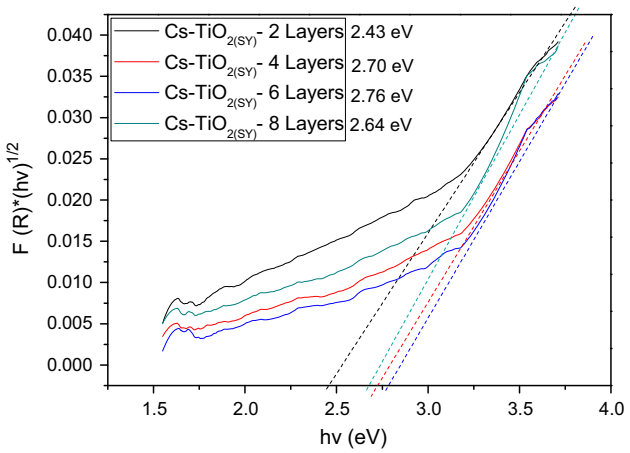

Fig. 4 UV-DR spectra of Cs–$TiO_{2(SY)}$/glass substrate multilayers photocatalyst which are 2, 4, 6, and 8 layers

band gap of the 8-layer photocatalyst for Cs–$TiO_{2(SY)}$/glass substrate is 2.64 eV. It was also demonstrated that the 8-layer photocatalyst of Cs–TiO_2/glass substrate was prepared by successive deposition cycles to guarantee the excellent distribution of nano-$TiO_{2(SY)}$. This, in turn, renders the Cs–$TiO_{2(SY)}$/glass substrate multilayer photocatalyst system, with the capability of absorbing photonic energy with wavelengths under 391 nm in the reflectance analysis.

Therefore, in this case, the coupled multilayer photocatalyst of Cs–$TiO_{2(SY)}$/glass substrate is expected to give higher adsorption–photodegradation efficiency than single TiO_2 in total removal of MO.

The morphology of Cs–TiO_2/glass substrate multilayer photocatalyst with distribution, surface structure, and homogeneity of nano-$TiO_{2(SY)}$ within Cs matrix was analyzed using the FESEM. Figure 5 illustrates the FESEM micrographs of Cs–$TiO_{2(SY)}$/glass substrate multilayer photocatalyst. These series of dipping samples were prepared for Cs–$TiO_{2(SY)}$ photocatalyst. The FESEM micrographs of Cs–$TiO_{2(SY)}$/glass substrate with similar weight ratio of 2:2 (0.25 g of Cs:0.25 g of TiO_2) were shown for $TiO_{2(SY)}$. These series of dipping photocatalyst were prepared for Cs–$TiO_{2(SY)}$ photocatalyst. Generally, all multilayer photocatalysts demonstrated a macroreticular structure with a spherical primary nano-$TiO_{2(SY)}$ with a particle size of 10–30 nm. The photocatalyst of Cs–$TiO_{2(SY)}$/glass substrate was more homogeneous and dispersed uniformly until the number of layers became 8.

EDS is an analytical technique used for elemental analysis or chemical characterization. Overall, Table 2 shows the EDS analysis of element weight percent for all the elements present in the Cs–$TiO_{2(SY)}$/glass substrate, resulting in a total of 100 wt%. The analysis indicates the coexistence of Si, C, O, Ti, and N elements. It has confirms that the photocatalysis with number of layers of 2 and 8 Cs–$TiO_{2(SY)}$/glass substrate obtained the weight ratio of O to TiO_2 is 6:1. The multilayers proved that the one with the lesser multilayers tends to have less amounts of TiO_2 and Cs bonds compared to those with higher number of layers. Furthermore, the photocatalysts, from 2 to 8 layers of Cs–$TiO_{2(SY)}$/glass substrate, demonstrated an increment in the amount of O and Ti elements. Besides that, Si has been reduced for Cs–$TiO_{2(SY)}$/glass substrate from 2 to 8 layers.

This suggests that TiO_2 was successfully distributed within the Cs matrix via coordinate covalent bonding. Bond formation are possible between the Cs via metal ions. The formation would take place between –OH group (obtain from Cs) and Ti^{4+} (obtain from TiO_2). Furthermore the –NH_2 group of Cs produces hydrogels that can be used for attachment to a glass substrate. In the meantime, the NH_2 group of Cs produces hydrogels that can be used for attachment to a glass substrate. Moreover, $TiO_{2(SY)}$ was

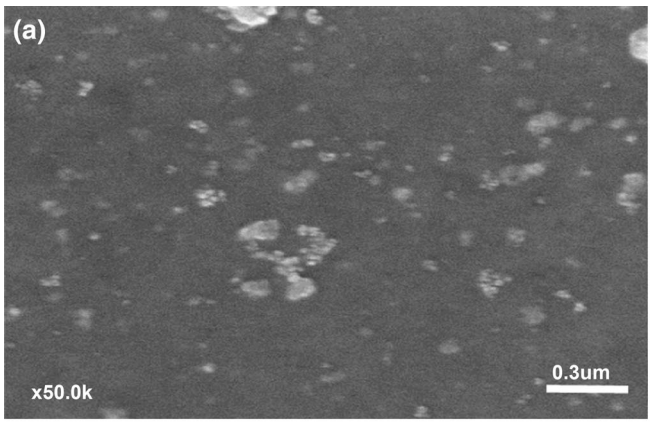

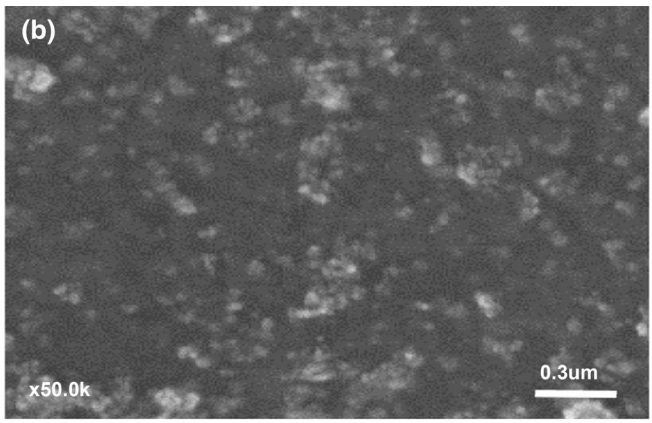

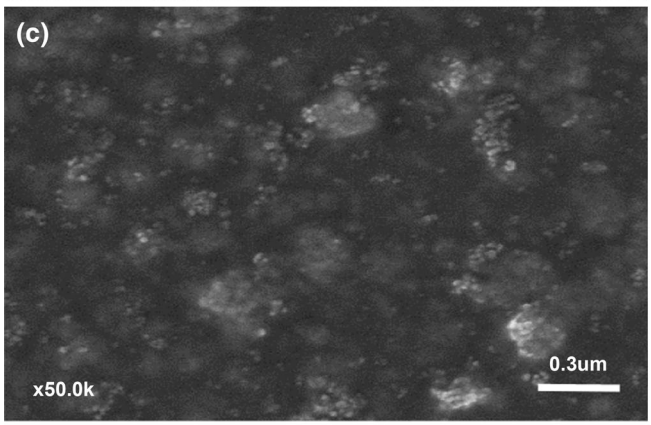

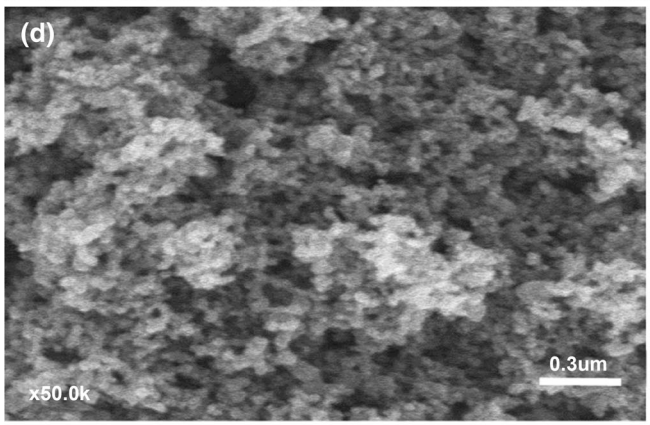

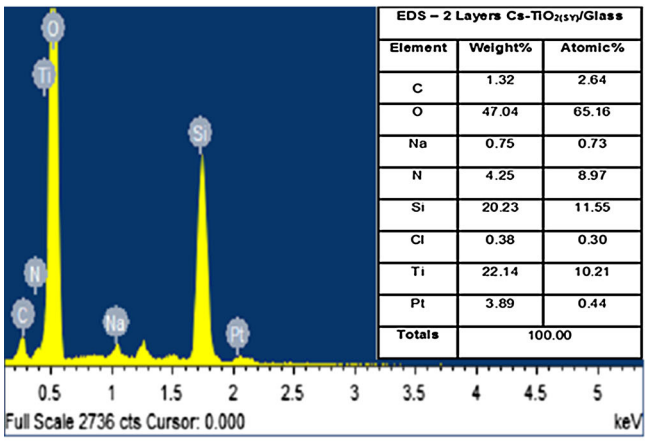

EDS – 2 Layers Cs-$TiO_{2(SY)}$/Glass

Element	Weight%	Atomic%
C	1.32	2.64
O	47.04	65.16
Na	0.75	0.73
N	4.25	8.97
Si	20.23	11.55
Cl	0.38	0.30
Ti	22.14	10.21
Pt	3.89	0.44
Totals	100.00	

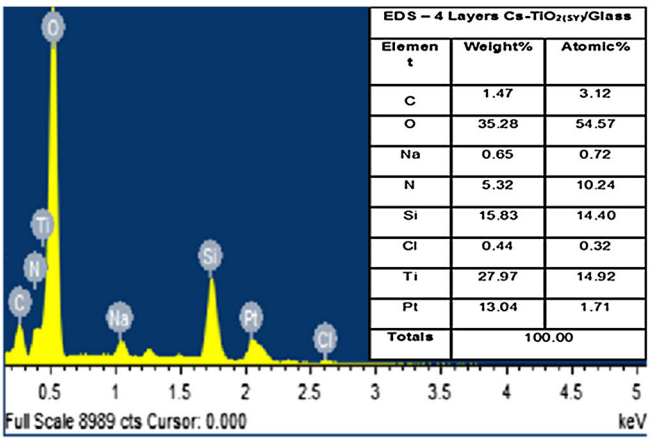

EDS – 4 Layers Cs-$TiO_{2(SY)}$/Glass

Element	Weight%	Atomic%
C	1.47	3.12
O	35.28	54.57
Na	0.65	0.72
N	5.32	10.24
Si	15.83	14.40
Cl	0.44	0.32
Ti	27.97	14.92
Pt	13.04	1.71
Totals	100.00	

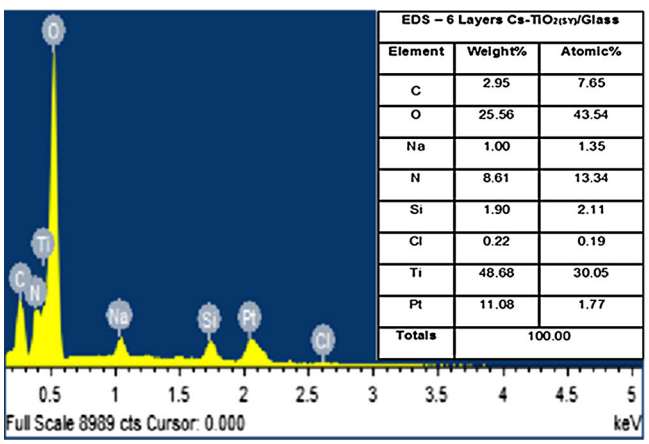

EDS – 6 Layers Cs-$TiO_{2(SY)}$/Glass

Element	Weight%	Atomic%
C	2.95	7.65
O	25.56	43.54
Na	1.00	1.35
N	8.61	13.34
Si	1.90	2.11
Cl	0.22	0.19
Ti	48.68	30.05
Pt	11.08	1.77
Totals	100.00	

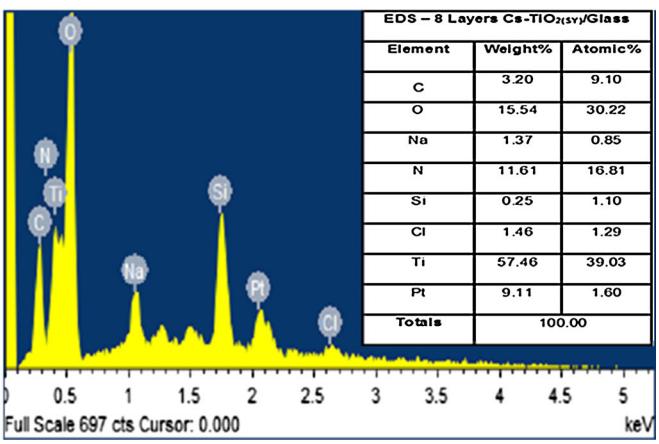

EDS – 8 Layers Cs-$TiO_{2(SY)}$/Glass

Element	Weight%	Atomic%
C	3.20	9.10
O	15.54	30.22
Na	1.37	0.85
N	11.61	16.81
Si	0.25	1.10
Cl	1.46	1.29
Ti	57.46	39.03
Pt	9.11	1.60
Totals	100.00	

◀**Fig. 5** FESEM micrographs of multilayer photocatalyst **a** 2 layers, **b** 4 layers, **c** 6 layers, **d** 8 layers of Cs–$TiO_{2(SY)}$/glass substrate with magnification of ×50,000 include with EDS figures and tables for that samples, respectively

Table 2 EDS of Cs–$TiO_{2(SY)}$/glass substrate multilayer photocatalyst that is relative to layer formations

Samples	Elements' weight percentage (%)				
	C	O	N	Si	Ti
Cs–$TiO_{2(SY)}$/glass substrate					
2 layers	1.32	47.04	4.25	20.23	22.14
4 layers	1.47	35.28	5.32	15.83	27.97
6 layers	2.95	25.56	8.61	1.90	48.68
8 layers	3.20	15.54	11.61	0.25	57.46

completely dispersed as the nanoparticles were submerged into the coated layers. Further observation leads us to conclude that the surface nano-$TiO_{2(SY)}$ was directly proportional to the number of layers. This would allow the Cs matrix to function as an adsorption medium, while the surface of $TiO_{2(SY)}$ acts as a photoelectron center via promotion and excitation with light illumination of a suitable wavelength. Hence, this confirmed that the photodegradation process plays a major role in 6–8 layers for Cs–$TiO_{2(SY)}$/glass substrate, due to the abundance of $TiO_{2(SY)}$, whereas the removal of MO would predominantly be attributed to the adsorption process by Cs.

Photocatalytic activity of MO adsorption–photodegradation

The UV–Vis analysis was carried out to quantitatively analyze the photocatalytic activities of Cs–$TiO_{2(SY)}$/glass substrate multilayer photocatalyst by relying on the MO photodegradation and including adsorption process. The adsorption–photodegradation activity of Cs–$TiO_{2(SY)}$/glass substrate toward 10 ppm of MO as a model of pollutant compound with layers of 2, 4, 6, and 8 is shown in Fig. 6. Approximately 50 % of the MO was adsorbed at initial stage (15-min adsorption in dark condition) and followed by the photodegradation (60-min degradation with UV light irradiation). The photocatalytic activities of Cs–$TiO_{2(SY)}$/glass substrate were analyzed based on the percentage of adsorption–photodegradation and final concentrations of MO. Firstly, photocatalyst with 2 layers showed the lowest MO adsorption about 30 %. With that, the remainder of MO concentration at 15 min of adsorption process was recorded to be 7.0 ppm. As far as photodegradation is concerned, 2-layer photocatalyst was

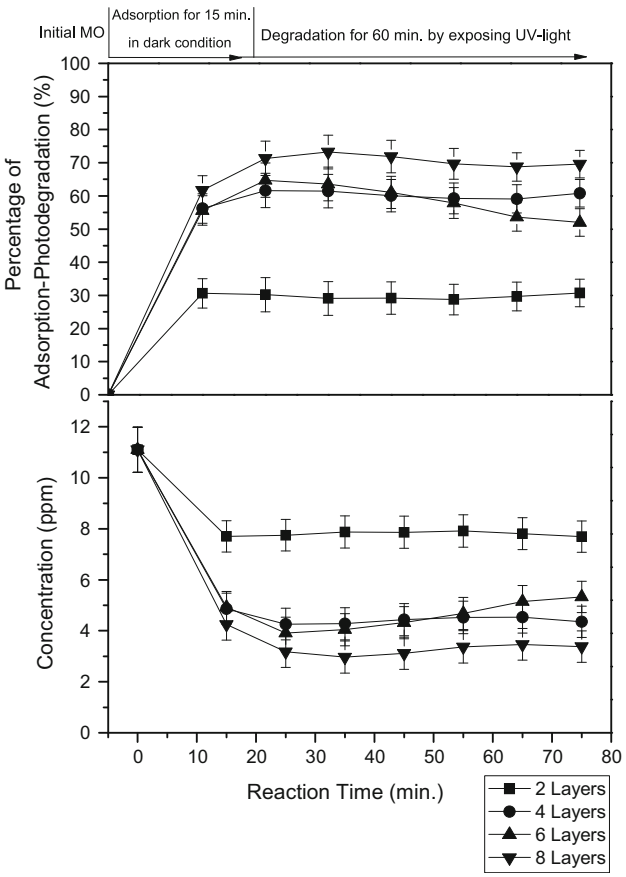

Fig. 6 Adsorption and photodegradation of Cs–$TiO_{2(SY)}$/glass substrate multilayer photocatalyst

recorded to be 30 % at 6.4 ppm of MO remaining. The adsorption and photodegradation processes improved as the layers increased from 4 to 8. The 4-layer photocatalyst results in about ~50 % MO adsorption with total removal of 5.0 ppm. The introduction of UV light resulted in an MO photodegradation of 61 %, at final concentrations of 4.3 ppm of MO by Cs–$TiO_{2(SY)}$/glass substrate. The MO adsorption for the photocatalyst of 6 layers was recorded to be 56 %, removing a total of 4.8 ppm of MO. However, the photodegradation did not show much difference in terms of percentage and concentrations of MO.

Furthermore, the 8 layers of Cs–$TiO_{2(SY)}$/glass substrate demonstrated the highest total removal of the MO. At the adsorption stage, 65 % of MO removal with final concentrations of 4.0 ppm for Cs–$TiO_{2(SY)}$/glass substrate is removed. Then, the photodegradation process was recorded to be 67–70 % removal. Once the process of photocatalytic activity was completed, the concentration of the remaining MO was recorded to be 3.4 ppm. This can be explained by the fact that samples with more layers contain higher percentages of Cs as its absorbent and TiO_2 as its center of photodegradation. This can be further explained by

Table 3 List of different photocatalysts with support of carbon as adsorbent in photocatalyst system to stimulate removal toward different pollutants

TiO_2 photocatalyst system	Pollutants	Removal (%)	References
Multiwall carbon nanotubes (MWCNTs)/nano-iron oxide	Chromium	90	Gupta et al. (2011a)
Alumina-coated carbon nanotubes	Lead	More than 99	Gupta et al. (2011b)
Multiwall carbon nanotubes (MWCNTs)/MnO_2	Arsenic	More than 95	Saleh et al. (2011)
Multiwall carbon nanotubes (MWCNTs)/ZnO	Cyanide	90	Saleh et al. (2010)

adsorption occurred on the inter-H-bonds interaction between the –OH and –NH_2 groups of Cs, with the polar groups of MO.

Thus, the MO removal is influenced by number of layers in photocatalyst system. The reason for MO molecular adsorption is derived from the Cs forms chelation between NH_2–MO and molecules–NH_2 within its long-chain structure. Interestingly, adsorption capability increases with increasing Cs–$TiO_{2(SY)}$ photocatalyst loading into glass substrate from 2 until 8 layers. It is evident that adsorption capability of Cs had not reached its maximum limit (Zainal et al. 2009). It can be explained that the sample with more layers contains high percentage of Cs as adsorbent and $TiO_{2(SY)}$ as a center for the photodegradation. The adsorption occurred via the inter-H-bonds interaction between the –OH and –NH_2 groups of Cs with the polar groups of MO. Once the MO has been introduced into the photocatalyst system, the reduction in MO would consequently occur by the photooxidation process which resulted in CO_2 and CO. Moreover, Table 3 shows several convenient interdisciplinary studies using different metal oxides with carbon as its adsorbent. It concluded that high levels of removal toward the selected pollutants is observed with different types of carbon support materials.

Mechanism of MO adsorption–photodegradation

FTIR is a useful analysis that helps identify types of functional groups of photocatalysts that are responsible for entrapping the molecules of dye, as illustrated in Fig. 7. Apparently, the presence of functional groups on adsorption site could be realized by NH_2, NH, and OH functional groups, together with TiO_2 metal oxide. Series of functional groups help confirm the effective removal of MO throughout the adsorption–photodegradation process. The process resulted in some changes from the interaction between the photocatalyst system and the MO solution. First, the presence of $TiO_{2(SY)}$ molecule was proven by the presence of strong absorbance bands at 498 cm^{-1}, with a shoulder at 680 cm^{-1}. In the absorption band at 3745 cm^{-1}, the spectral transmittance also appears as sharper bands for Cs–$TiO_{2(SY)}$ photocatalyst, indicating that –OH groups of Cs have been attached to TiO_2 network

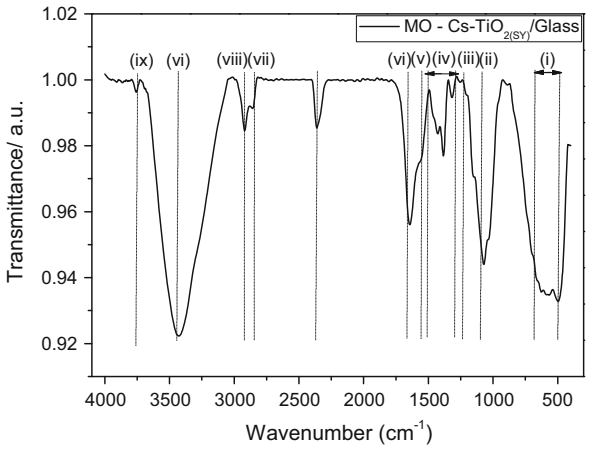

Symbol	Wavelength (cm^{-1})	Assignment
(i)	498 to 680	TiO_2 with shape of 8 layers formation with Cs
(ii)	1081	S=O vibration
(iii)	1315	–C=N stretching of MO
(iv)	1490 to 1280	Stretching bands of –NH_2 from Cs to be attached with –CH_3 from MO
(v)	1535	C–N and C–N–H mode of Cs
(vi)	1660	N-H bending vibration in –NH_2 group of Cs
(vi)	3420	–OH groups of Cs
(vii)	2850	OH bands of surface TiO_2-OH functional groups
(viii)	2920	–C–H stretching
(ix)	3745	Indicating that –OH groups of Cs to be attached with TiO_2 network

Fig. 7 FTIR spectra of MO with 8-layer photocatalyst of Cs–$TiO_{2(SY)}$/glass substrate after photocatalytic activities

(Fajriati et al. 2014). Furthermore, the adsorption bands of Cs were measured at 3420 and 1660 cm^{-1}, which was assigned to its –OH (mostly adsorption toward TiO_2) and –NH_2 (mostly adsorption toward MO) functional groups. Moreover, the multilayer photocatalyst on the Cs–$TiO_{2(SY)}$/glass substrate is related to the enhanced permeated pure water via the polarity –OH and can interact with water molecules through van der Waals force and H-bond (Saleh and Gupta 2012b). Furthermore, Cs mode can be confirmed via the band at 1535 cm^{-1}, which help identify the functional groups of –C–N and C–N–H, while bands of –NH and C=O have also been observed at 1660 cm^{-1} (Kavitha et al. 2013).

The effectiveness of the photocatalytic reaction hinges more on the adsorption rather than on photodegradation process, due to the present amount of MO molecules after the completion of the photocatalytic reaction. There are some new spectrum bands (MO functional groups) appearing, which is obvious post-analysis. Moreover, MO molecules are detectable after absorption by Cs molecules. The band at 1660 cm^{-1} was clearly weakened after the photodegradation process, which might be due to $–NH_2$ groups in its role of absorbing MO. The range of bending attributed to the –C=N stretching was observed at 1315 cm^{-1}, while C=C stretching at 1660 cm^{-1} was observed between the binding of Cs and MO. Most of adsorption functional groups of Cs have been identified from 1490 to 1280 cm^{-1}, attributed to the existence of protonated $–NH_2$ groups in the Cs structure, forming H-bonds with the $–CH_3$ site from the MO molecule. In a nutshell, most MO molecules can be obtained from the adsorption process via Cs. The interaction of MO molecules with the photocatalyst could be demonstrated at 1380 cm^{-1}, which shows the stretching of C–C and N=N vibrations, respectively. The aromatic –C–H stretching band at 2920 cm^{-1} indicates the presence of MO molecules within the photocatalyst. Furthermore, the spectra were recorded in the form of a strong increase in absorbance level below 1081 cm^{-1}, representing the stretching of –S=O functional groups. Confirmation with the characteristics of MO molecules was at 1081 cm^{-1} –S=O stretching vibrations, 2920 cm^{-1} –CH stretching, and 1315 cm^{-1} –C=N stretching (Nandini and Vishalakshi 2012). The band around 2360 cm^{-1} (the line without label) was not characteristic of Cs–$TiO_{2(SY)}$ photocatalyst, or even MO, but was due to CO_2, which might affect calculations.

Conclusion

In this study, the photocatalytic activity for the total removal of MO solution was determined using multilayer photocatalyst of Cs–$TiO_{2(SY)}$/glass substrate. The HR-TEM analysis of $TiO_{2(SY)}$ showed an average homogenous dispersion and uniform particulate features with average particle sizes of 13.3 nm. The Cs–$TiO_{2(SY)}$/glass substrate showed good homogenous dispersion, binding ability, and interfaces, as determined from FTIR, FESEM, and EDS analyses. The UV-DR analysis showed that all photocatalyst samples have lowest band gap of under 3.0 eV. The results indicated that 8-layer photocatalysts resulted in the optimal adsorption–photodegradation Cs–$TiO_{2(SY)}$/glass substrate, with the adsorption–photodegradation of 70 % and adsorption of 50 % of the MO solution.

Acknowledgments This work is financially supported by Fundamental Research Grant Scheme (FRGS: FP049-2013B) by University of Malaya and Ministry of High Education (MOE), Malaysia.

References

Ali I (2010) The quest for active carbon adsorbent substitutes: inexpensive adsorbents for toxic metal ions removal from wastewater. Sep Purif Rev 39(3–4):95–171

Ali I (2012) New generation adsorbents for water treatment. Chem Rev 112(10):5073–5091

Ali I (2014) Water treatment by adsorption columns: evaluation at ground level. Sep Purif Rev 43(3):175–205

Ali I, Asim M, Khan TA (2012) Low cost adsorbents for the removal of organic pollutants from wastewater. J Environ Manag 113:170–183

Bagheri S, Mohd Hir ZA, Termeh Yousefi A, Abd Hamid SB (2015) Photocatalytic performance of activated carbon-supported mesoporous titanium dioxide. Desalination Water Treat 1–7. doi:10.1080/19443994.2015.1038593

Dutta PK, Dutta J, Tripathi VS (2004) Chitin and chitosan: chemistry, properties and applications. J Sci Ind Res 63(1):20–31

Fajriati I, Mudasir M, Wahyuni ET (2014) Photocatalytic decolorization study of methyl orange by TiO_2–chitosan nanocomposites. Indones J Chem 14(3):209–218

Fujishima A (1972) Electrochemical photolysis of water at a semiconductor electrode. Nature 238:37–38

Gupta VK, Agarwal S, Saleh TA (2011a) Chromium removal by combining the magnetic properties of iron oxide with adsorption properties of carbon nanotubes. Water Res 45(6):2207–2212

Gupta VK, Agarwal S, Saleh TA (2011b) Synthesis and characterization of alumina-coated carbon nanotubes and their application for lead removal. J Hazard Mater 185(1):17–23

Gupta VK, Jain R, Mittal A, Saleh TA, Nayak A, Agarwal S, Sikarwar S (2012) Photo-catalytic degradation of toxic dye amaranth on TiO_2/UV in aqueous suspensions. Mater Sci Eng C Mater Biol Appl 32(1):12–17

Jawad AH, Nawi M (2012) Fabrication, optimization and application of an immobilized layer-by-layer TiO_2/chitosan system for the removal of phenol and its intermediates under 45-W fluorescent lamp. React Kinet Mech Catal 106(1):49–65

Kavitha K, Sutha S, Prabhu M, Rajendran V, Jayakumar T (2013) In situ synthesized novel biocompatible titania–chitosan nanocomposites with high surface area and antibacterial activity. Carbohydr Polym 93(2):731–739

Kijima T (2010) Inorganic and metallic nanotubular materials: recent technologies and applications, vol 117. Springer, Berlin

Kim TY, Lee Y-H, Park K-H, Kim SJ, Cho SY (2005) A study of photocatalysis of TiO_2 coated onto chitosan beads and activated carbon. Res Chem Intermed 31(4):343–358

Kyzas GZ, Bikiaris DN (2015) Recent modifications of chitosan for adsorption applications: a critical and systematic review. Mar Drugs 13(1):312–337

Liu H, Ramnarayanan R, Logan BE (2004) Production of electricity during wastewater treatment using a single chamber microbial fuel cell. Environ Sci Technol 38(7):2281–2285

Nandini R, Vishalakshi B (2012) A study of interaction of methyl orange with some polycations. J Chem 9(1):1–14

Pereira L, Alves M (2012) Dyes—environmental impact and remediation. In: Environmental protection strategies for sustainable development. Springer, pp 111–162

Qian T, Su H, Tan T (2011) The bactericidal and mildew-proof activity of a TiO_2–chitosan composite. J Photochem Photobiol A 218(1):130–136

Saleh TA, Gupta VK (2012a) Photo-catalyzed degradation of hazardous dye methyl orange by use of a composite catalyst consisting of multi-walled carbon nanotubes and titanium dioxide. J Colloid Interface Sci 371(1):101–106

Saleh TA, Gupta VK (2012b) Synthesis and characterization of alumina nano-particles polyamide membrane with enhanced flux rejection performance. Sep Purif Technol 89:245–251

Saleh TA, Gondal MA, Drmosh QA (2010) Preparation of a MWCNT/ZnO nanocomposite and its photocatalytic activity for the removal of cyanide from water using a laser. Nanotechnology 21(49):495705

Saleh TA, Agarwal S, Gupta VK (2011) Synthesis of MWCNT/MnO_2 and their application for simultaneous oxidation of arsenite and sorption of arsenate. Appl Catal B 106(1):46–53

Wongkupasert S (2008) The effect of salt form and molecular weight of chitosan for efficiency on siRNA delivery into cell. Silpakorn University, Bangkok

Yao K, Li J, Yao F, Yin Y (2011) Chitosan-based hydrogels: functions and applications. CRC Press, Boca Raton

Yu X, Lu Z, Wu D, Yu P, He M, Chen T et al (2014) Heteropolyacid–chitosan/TiO_2 composites for the degradation of tetracycline hydrochloride solution. React Kinet Mech Catal 111(1):347–360

Zainal Z, Hui LK, Hussein MZ, Abdullah AH, Hamadneh IM (2009) Characterization of TiO_2–chitosan/glass photocatalyst for the removal of a monoazo dye via photodegradation–adsorption process. J Hazard Mater 164(1):138–145

Zhang X, Zhao X, Su H (2011) Degradation characteristic of TiO_2–chitosan adsorbent on rhodamine B and purification of industrial wastewater. Korean J Chem Eng 28(5):1241–1246

Zhu H, Jiang R, Fu Y, Guan Y, Yao J, Xiao L, Zeng G (2012) Effective photocatalytic decolorization of methyl orange utilizing TiO_2/ZnO/chitosan nanocomposite films under simulated solar irradiation. Desalination 286:41–48